**RAA 2015** Vol. **15** No. **8**, 1438–1448 doi: 10.1088/1674–4527/15/8/023
*http://www.raa-journal.org* *http://www.iop.org/journals/raa*

*Research in Astronomy and Astrophysics*

# The LAMOST survey of background quasars in the vicinity of M31 and M33 – III. results from the 2013 regular survey

Zhi-Ying Huo[1], Xiao-Wei Liu[2], Mao-Sheng Xiang[2], Jian-Rong Shi[1], Hai-Bo Yuan[3] ⋆, Yang Huang[2], Yong Zhang[4], Yong-Hui Hou[4], Yue-Fei Wang[4] and Ming Yang[1]

[1] National Astronomical Observatories, Chinese Academy of Sciences, Beijing 100012, China; *zhiyinghuo@bao.ac.cn*
[2] Department of Astronomy, Peking University, Beijing 100871, China
[3] Kavli Institute for Astronomy and Astrophysics, Peking University, Beijing 100871, China
[4] Nanjing Institute of Astronomical Optics & Technology, Chinese Academy of Sciences, Nanjing 210042, China

Received 2015 March 30; accepted 2015 May 8

**Abstract** In this work, we report new quasars discovered in fields in the vicinity of the Andromeda (M31) and Triangulum (M33) galaxies with the Large Sky Area Multi-Object Fiber Spectroscopic Telescope (LAMOST, also called the Guo Shou Jing Telescope) during the 2013 observational season, the second year of the regular survey. In total, 1330 new quasars are discovered in an area of $\sim$133 deg$^2$ around M31 and M33. With $i$ magnitudes ranging from 14.79 to 20.0 and redshifts from 0.08 to 4.85, the 1330 new quasars represent a significant increase in the number of identified quasars in fields in the vicinity of M31 and M33. Up to now, there have been a total of 1870 quasars discovered by LAMOST in this area. The much enlarged sample of known quasars in this area can potentially be utilized to construct a precise astrometric reference frame for the measurement of minute proper motions of M31, M33 and their associated substructures, which are vital for understanding the formation and evolution of M31, M33 and the Local Group of galaxies. Moreover, in the sample, there are a total of 45, 98 and 225 quasars with $i$ magnitudes brighter than 17.0, 17.5 and 18.0 respectively. In the aforementioned brightness bins, 15, 35 and 84 quasars are reported here for the first time, and 6, 21 and 81 are reported in our pervious work. In addition, 0, 1 and 6 are from the Sloan Digital Sky Survey and 24, 41 and 54 are from the NED database. These bright quasars provide an invaluable sample to study the kinematics and chemistry of the interstellar/intergalactic medium of the Local Group.

**Key words:** galaxies: individual (M31, M33) — quasars: general — quasars: emission lines

## 1 INTRODUCTION

Since the first optical spectral identifications of a quasar (Schmidt 1963), the number of known quasars has steadily and rapidly increased. In particular, the Sloan Digital Sky Survey (SDSS; York

⋆ LAMOST Fellow.

et al. 2000) has currently discovered about ∼260 000 quasars (see Schneider et al. 2010; Pâris et al. 2012, 2014 and references therein). Being the most energetic objects in the universe, quasars have been widely used as excellent tracers to study a variety of astrophysical problems, such as the large scale structure of the universe (e.g. Boyle et al. 2000), central massive black holes of galaxies (e.g. Corbett et al. 2003), galaxy formation and evolution (e.g. Gebhardt et al. 2000), and the interstellar/intergalactic medium (ISM/IGM) (e.g. Murdoch et al. 1986; Savage et al. 2000).

The Andromeda galaxy (M31) is the most luminous member of the Local Group of galaxies and the nearest archetypical spiral galaxy that serves as one of the best astrophysical laboratories for studies of the formation and evolution of galaxies. The deep photometric surveys performed by the Canada-France-Hawaii Telescope (Ibata et al. 2007; McConnachie et al. 2009) have revealed a large variety of complex substructures within hundreds of kiloparsecs (kpc) of M31, with some extending all the way to the Triangulum galaxy (M33), pointing toward a possible encounter between these two galaxies in the past. Further chemical and kinematic investigations of M31, M33 and associated substructures are vital for understanding the assembly history of the Local Group.

With a distance of $\sim$ 785 kpc (McConnachie et al. 2005), M31 is moving towards the Milky Way at a speed of 117 km $s^{-1}$ (Binney & Tremaine 1987). Moreover, its transverse velocity has remained unmeasurable for a long time. The distance and proper motion (PM) of M33 have been measured by the Very Long Baseline Array (Brunthaler et al. 2005). Nevertheless, water maser sources in M31 have been discovered only recently (Darling 2011) and so do not yet have a long enough time baseline for accurate PM measurements. Based on the kinematics of M33 and IC 10, two satellite galaxies of M31, Loeb et al. (2005) and van der Marel & Guhathakurta (2008) present theoretical estimates of the PM of M31, about 80 km $s^{-1}$ (20 μas $yr^{-1}$). Based on Hubble Space Telescope (HST) imaging data spanning 5–7 years, Sohn et al. (2012) present the first direct PM measurements of three M31 fields, each with an area of $\sim 2.7\times2.7$ $arcmin^2$. Due to the sparsity of known background quasars, compact background galaxies are used instead as reference sources for the PM measurements. Given the importance of PM measurements for understanding the kinematics of M31, M33 and those associated structures, securing a sufficiently large number and density of background quasars would be extremely useful for constructing an accurate reference frame for precise PM measurements.

A series of studies based on the Spectroscopic and Photometric Landscape of Andromeda's Stellar Halo (SPLASH; see Dorman et al. 2012; Gilbert et al. 2009, 2012, 2014; Tollerud et al. 2012 and reference therein) survey present the kinematical and chemical properties of stars in M31 and its extended halos, as well as in features of tidal debris and dwarf galaxies. Spectroscopic measurements of the chemical composition of stars at the distance of M31 are not easy tasks even for ten-meter class telescopes, including Keck. Absorption-line spectroscopy of bright quasars in fields in the vicinity of M31 and M33 can be used to probe the chemical composition, distribution and kinematics of the ISM/IGM associated with the Milky Way, M31, M33 and related substructures. Several studies published hitherto (see Savage et al. 2000; Schneider et al. 1993 and references therein), based on data collected with the Hubble Space Telescope Quasar Absorption Line Key Project have revealed a wide range of ionization states, chemical compositions and kinematics of gas in the Milky Way halo. Rao et al. (2013) studied the properties of the extended gas halo of M31 using observations of 10 background quasars with the HST Cosmic Origins Spectrograph (COS). Such studies are however currently limited to a few lines of sight and restricted by the available number of bright (low-redshift) quasars in the fields of interest.

The Large Sky Area Multi-Object Fiber Spectroscopic Telescope (LAMOST) is an innovative reflecting Schmidt telescope with a design allowing both a large light-collecting aperture (with the effective aperture varying between 3.6 m–4.9 m, depending on the declination and hour angle of pointing) and a wide field of view of 5 degrees in diameter (Cui et al. 2012; Wang et al. 1996; Su & Cui 2004). With a spectral resolution of R $\approx$ 1800 and a wavelength coverage of 3700–9000 Å, LAMOST can simultaneously record spectra of up to 4000 celestial objects. After commissioning

for two years (2009–2010) and the pilot survey that lasted one year (2011), the LAMOST regular survey was initiated in October 2012 (Zhao et al. 2012).

This is the third installment presenting the results of the LAMOST survey of background quasars in fields in the vicinity of M31 and M33. In the first paper of this series, we reported 14 new quasars discovered with LAMOST using the early commissioning data collected in 2009 (Huo et al. 2010, hereafter Paper I). In the second paper, we presented 526 newly discovered quasars, based on data collected during the 2010 commissioning as well as the 2011 pilot survey (Huo et al. 2013, hereafter Paper II). In this paper, we present newly discovered background quasars in this area in the 2013 observational season, the second year of the regular survey.

The paper is organized as follows. In Section 2, we present quasar candidate selection. Observations and data reduction are described in Section 3. The quasar sample and its properties are described in Section 4.

## 2 CANDIDATE SELECTION

Quasar candidates are selected based on the optical and near infrared (IR) photometric data available in fields in the vicinity of M31 and M33. Within the SDSS coverage, low-redshift quasar candidates are selected by following Richards et al. (2002). Quasar candidates and stars are well separated in the SDSS color-color diagrams. Candidates down to an $i$-band magnitude limit of 20.0 mag (with a surface number density of $\sim$27 candidates per square degree) are selected (see Papers I and II for more details). In the central area of M31 and M33, no reliable photometric data are provided by the SDSS as well as the Xuyi Schmidt Telescope Photometric Survey (XSTPS; Liu et al. 2014). Quasar candidates are selected using data from the Kitt Peak National Observatory (KPNO) 4 m telescope survey of M31 and M33 (Massey et al. 2006), after transforming the KPNO $UBVRI$ magnitudes to SDSS $ugriz$ magnitudes using the transformation of Jester et al. (2005) deduced for quasars with redshifts $z \leq 2.1$.

In addition to the optically selected candidates, the Wide-field Infrared Survey Explorer (WISE; Wright et al. 2010) sources with colors $W1 - W2 \geq 0.8$ are selected as candidates (Yan et al. 2013, Stern et al. 2012). The IR sources are cross-correlated with the available optical point-source catalogs of SDSS, KPNO and XSTPS (see Paper II for more details). By this method, about 26 candidates per square degree are selected down to a limiting magnitude of $i \leq 20.0$ mag. As shown in Wu et al. (2012), this IR-based selection is capable of finding quasars with redshifts up to $z < 3.5$. Figure 1 shows the sky coverage of SDSS and XSTPS in the area of M31 and M33.

## 3 OBSERVATIONS AND DATA REDUCTION

The quasar candidates in fields in the vicinity of M31 and M33 have been targeted by LAMOST since its initial commissioning in 2009; see Paper I and Paper II for the previous results on quasars discovered with LAMOST in this area. Here we report results based on data collected in the 2013 observational season, the second year of the LAMOST regular survey. Through two years (2009–2010) of commissioning, one year (2011) of the pilot survey and one year (2012) of the regular survey we have seen that the performance of LAMOST has been stabilized, with some steady improvement over time (Huo et al. 2015, in preparation; Yuan et al. 2015, in preparation). There are dozens of papers published based on the LAMOST data, see the preface of this special issue (Liu et al. 2015).

There are 10 plates with quasar candidates observed by LAMOST in the 2013 observational season. Similar to the LAMOST Spectroscopic Survey of the Galactic Anti-center (LSS-GAC; Liu et al. 2014; Yuan et al. 2015 for detail), three categories of spectroscopic plates are designated, bright (B), medium (M) and faint (F), targeting sources with different brightnesses for efficient usage of observing times that have different qualities while also avoiding fiber cross-talk. All quasar candidates are only assigned to fibers in M plates regardless of their brightness, except for a few quasar candidates with $r$ magnitude brighter than 16.3. The latter have been assigned fibers in B

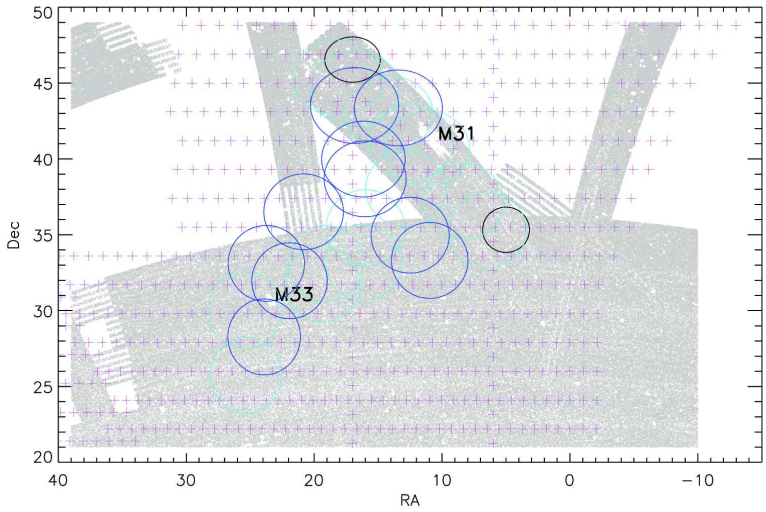


**Fig. 1** Sky coverage of the SDSS and XSTPS in the area of M31 and M33. The positions of M31 and M33 are marked. The grey area represents the SDSS sky coverage of this area. The magenta plus symbols delineate the individual field centers of the XSTPS M31/M33 survey, with each field covering an area of $2\times$ 2 deg$^2$. The black circles represent the three spectroscopic fields that target quasar candidates in the outer halo of M31 by SDSS; the one in the northeast area represents two fields with the same central positions. The cyan circles label the LAMOST fields observed in 2010 and 2011. The blue circles represent the LAMOST fields observed in the 2013 observational season.

plates and observed repeatedly. The exposure times for the individual M plates vary between 1800 to 2400 s, and are repeated two or three times for cosmic ray rejections and for buildup of the signal-to-noise ratio (SNR). The spectra have a wavelength coverage of 3700–9000 Å, with a resolving power of R $\approx$1800. In total, 7425 unique quasar candidates were targeted in the 2013 season, and some of them were targeted repeatedly. Because of the circular field of view of LAMOST, some overlap of the field is necessary in order to have contiguous sky coverage. See Figure 1 for the fields targeted by LAMOST in 2013.

The spectra were reduced with the LAMOST two-dimensional (2D) pipeline, version 2.6 (Luo et al. 2004, 2012, 2015). Given the relatively low throughputs of LAMOST at blue wavelengths, and the relative faintness of quasar candidates, flux-calibration often induces larger uncertainties. As such, for the purpose of identifying quasars of interest here, we use spectra without flux calibration.

## 4 RESULTS AND DISCUSSION

The current work is based on data collected during 2013, the second year of the LAMOST regular survey. The performance of LAMOST, including throughput and fiber positioning, improved significantly compared to earlier times when LAMOST was operating. Sky subtraction, although improved, is still not as good as expected, especially at wavelengths longer than 7200 Å. Fortunately, quasars are easily identified with their characteristic broad emission lines. We require that at least one emission line is securely identified. We visually examine the one-dimensional (1D) extracted spectra of quasar candidates one by one, and this leads to the identifications of 1545 quasars in the 10 observed fields near M31 and M33, 1370 of which are newly discovered. If we adopt a luminosity cut by following the SDSS Quasar Survey (Schneider et al. 2010, also see the references therein), with an absolute $i$-band magnitude of $M_i = -22.0$ in a cosmology with $H_0 = 70$ km s$^{-1}$ Mpc$^{-1}$, $\Omega_{\rm M} = 0.3$ and $\Omega_\Lambda = 0.7$, the number of identified quasars is 1503, of which 1330 are new.

**Table 1** Catalog of New Quasars in Fields in the Vicinity of M31 and M33 Discovered by LAMOST in the 2013 Observational Season

| Object | R.A. | Dec. (J2000) | Redshift | $u$ | $g$ | $r$ | $i$ | $z$ | A(i) | Selection* |
|---|---|---|---|---|---|---|---|---|---|---|
| J003234.36+335838.0 | 8.143199 | 33.977227 | 1.46 | 20.16 | 20.10 | 19.82 | 19.64 | 19.62 | 0.17 | W,S,– |
| J003237.68+330028.2 | 8.157018 | 33.007835 | 1.22 | – | 19.64 | 19.54 | 19.16 | – | 0.19 | W,–,– |
| J003238.14+331814.1 | 8.158927 | 33.303941 | 1.57 | 19.82 | 19.41 | 19.35 | 19.09 | 19.08 | 0.16 | W,S,– |
| J003326.08+322235.3 | 8.358672 | 32.376485 | 2.87 | 21.08 | 20.00 | 19.80 | 19.65 | 19.49 | 0.16 | W,–,– |
| J003333.87+331441.5 | 8.391137 | 33.244884 | 2.51 | 19.83 | 18.98 | 18.50 | 18.40 | 18.19 | 0.17 | W,–,– |
| J003347.28+340456.8 | 8.447031 | 34.082462 | 2.22 | – | 19.48 | 19.25 | 19.24 | – | 0.20 | W,–,– |
| J003354.78+335628.9 | 8.478290 | 33.941377 | 1.72 | 21.34 | 21.05 | 20.46 | 19.95 | 19.89 | 0.17 | W,–,– |
| J003437.21+334634.1 | 8.655059 | 33.776146 | 1.72 | 18.16 | 18.24 | 18.00 | 17.62 | 17.76 | 0.16 | W,S,– |
| J003445.88+333018.4 | 8.691207 | 33.505132 | 2.22 | – | 18.98 | 19.19 | 18.79 | – | 0.17 | W,–,– |
| J003459.55+323110.9 | 8.748138 | 32.519718 | 0.44 | 19.60 | 19.22 | 19.05 | 18.94 | 18.82 | 0.16 | W,S,– |
| ..... | ... | ... | | | | | | | | |

Notes: * W represents those candidates selected by the IR criteria based on the WISE data, S represents optically selected cases using the SDSS criteria for low-redshift quasars, and M represents optically selected cases from the KPNO data (Massey et al. 2006). Only part of Table 1 is shown here for illustration. The whole table contains information on 1330 new quasars is available on *http://www.raa-journal.org/docs/Supp/ms2222table1.txt*.

All the new quasars have reasonable SNRs and at least one emission line securely identified, allowing reliable redshift estimations (see Fig. 2). Table 1 presents the catalog of these newly discovered quasars, including target designation (in the format J*hhmmss.ss+ddmmss.s*), J2000.0 coordinates (right ascension (R.A.) and declination (Dec.) in decimal degrees), redshifts, the observed SDSS $u$, $g$, $r$, $i$ and $z$ magnitudes without extinction corrections, $i$-band extinction from Schlegel et al. (1998), and the selection criteria used. Only a portion of the table is shown here. The whole table containing information on 1330 new quasars is only available in the online electronic version. In the last column of Table 1, W indicates targets selected with the IR criteria based on the WISE data, S indicates targets selected using the SDSS criteria for low-redshift quasars, and M indicates those targets selected based on the KPNO data of the Local Group of galaxies. No quasars selected from the KPNO data are discovered in this 2013 observational season. Columns 5-9 list the SDSS $u$, $g$, $r$, $i$ and $z$ magnitudes. For some targets, the $u$ and $z$ magnitudes are not given. Those targets are selected by cross-matching the WISE IR candidates with the XSTPS optical catalog.

Figure 2 shows the LAMOST spectra of four new quasars with a wide range of properties. The spectra have not been flux-calibrated. At wavelengths shorter than 4000 Å where the instrument throughputs are relatively low, as well as between the dichroic crossover wavelength range 5700–6000 Å, the spectra have relatively low SNRs. Since the LAMOST spectra are oversampled, they are binned by a factor of 4 to improve the SNRs. Cosmic rays that remained after pipeline processing have been manually removed for clarity.

Here we present a brief description of the properties of the four quasars shown in Figure 2. At a redshift of 0.08 and with an $i$ magnitude of 14.79, J004342.54+372519.9 is the brightest quasar and the quasar with the lowest redshift in the catalog reported in this paper. With a redshift of 4.85, J012220.29+345658.4 is the quasar with the highest redshift presented here. It is also the quasar with the highest redshift discovered by LAMOST by the end of the 2013 observational season, as far as we know. This object was also observed in January of 2015 with the Yunnan Faint Object Spectrograph and Camera (YFOSC) mounted on the Lijiang 2.4 m telescope administered by Yunnan Astronomical Observatory. The identification and redshift initially found in the LAMOST spectrum were confirmed. J010508.48+440955.6 is an example of a quasar in our catalog with broad absorption lines, having an emission line redshift of 2.93. J004037.83+341859.2, at a redshift of $z = 2.70$ and an $i$-band absolute magnitude of $M_i = -30.19$ mag, is the most luminous quasar in our catalog.

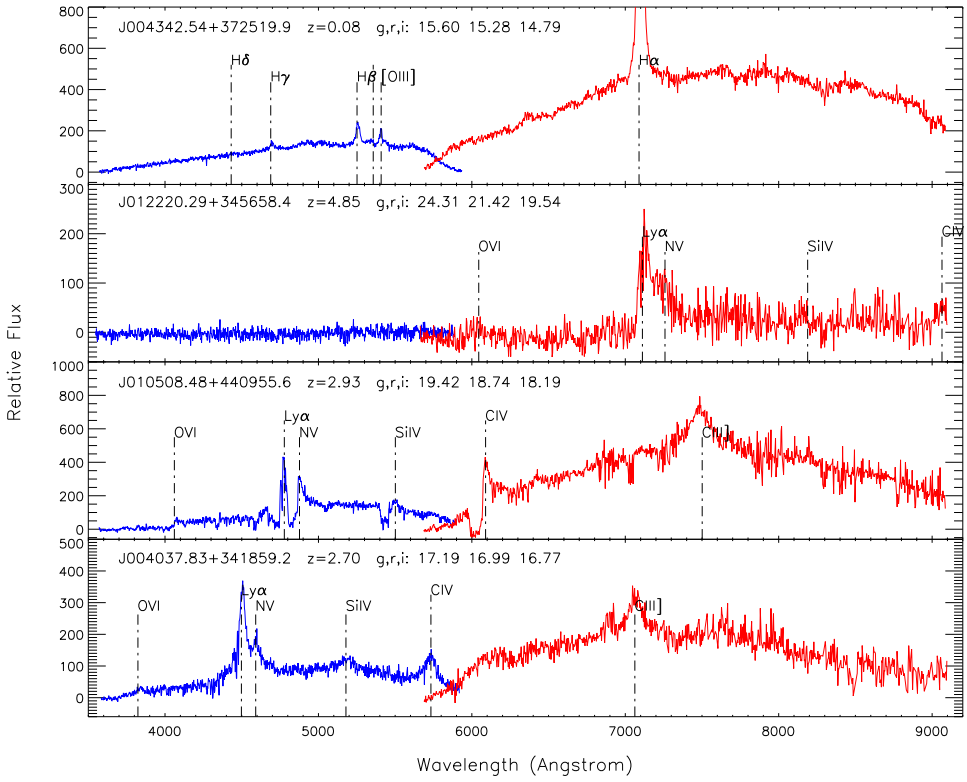


**Fig. 2** Examples of newly discovered quasars by LAMOST in the 2013 regular survey. The vertical dash-dotted lines label identified emission lines. The $y$-axis is the relative flux in units of counts per pixel. The spectra have been binned by a factor of 4, and cosmic rays that remained after pipeline processing were manually removed for clarity.

### 4.1 Spatial Distributions

The spatial distributions of all known background quasars in fields in the vicinity of M31 and M33 are shown in Figure 3, in the $\xi$–$\eta$ plane. Here $\xi$ and $\eta$ are respectively the R.A. and Dec. offsets relative to the optical center of M31 (Huchra et al. 1991). There are, in total, 1870 quasars discovered by LAMOST by the end of the 2013 observational season, including 1330 newly discovered quasars in an area of $\sim$133 deg$^2$ reported in this paper. In addition, there were 14 and 526 quasars discovered using earlier observations by LAMOST, as reported in Papers I and II, respectively. In addition, 75 quasars were identified in three SDSS spectroscopic plates in two fields in the outer halo of M31 along its major axis (Adelman-McCarthy et al. 2006, 2007), 43 quasars were discovered serendipitously in two Sloan Extension for Galactic Understanding and Exploration (SEGUE; Yanny et al. 2009) plates in this area, and 155 previously known quasars with redshifts were listed in the NED archive within 10° of M31 and of M33. In Figure 3, the central positions of M31 and M33 are marked by magenta stars. The magenta ellipse represents the optical disk of M31, with an optical radius of $R_{25} = 95.3'$ (de Vaucouleurs et al. 1991), an inclination angle of $i = 77°$ and a position angle of $PA$ =35° (Walterbos & Kennicutt 1987). The number of known quasars, behind the extended halo and substructures associated with M31, has increased by a substantial amount.

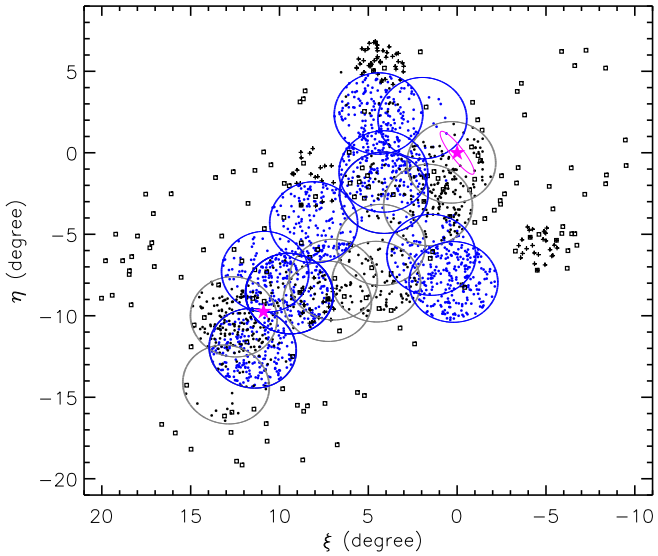


**Fig. 3** Spatial distributions of background quasars in fields in the vicinity of M31 and M33. Blue filled circles represent quasars identified by LAMOST in the 2013 dataset. Black filled circles represent quasars identified in the LAMOST 2009, 2010 and 2011 datasets. Pluses and open squares represent SDSS quasars and previously known quasars with redshifts given in the NED archive, respectively. The central positions of M31 and M33 are marked by the magenta stars, while the magenta ellipse represents the optical disk of M31 with radius $R_{25} = 95.3'$. The large grey and blue circles signify the locations of the LAMOST fields observed in 2011 and 2013, respectively.

The much enlarged number of known quasars in fields in the vicinity of M31 and M33 will serve as an invaluable sample for future PMs and ISM/IGM studies of M31, M33 and the Local Group.

The LAMOST quasars are mainly distributed around M31 and M33, as well as the area between M31 and M33, including the Giant Stellar Stream (see Fig. 3). However, the spatial distribution of quasars identified by LAMOST is not uniform. Of the 10 plates observed in 2013, five plates have 200 or more quasars that have been identified, one plate contains only 75 quasars that have been identified, while the remaining four plates have between 100 and 200 quasars that have been identified. The highest density of quasars identified by LAMOST in 2013 is $\sim$12.8 quasars per square degree. The overall efficiency of quasar identifications in the 2013 observational season is $\sim$21% (1545/7425), although the improvement is significant compared to what was achieved in Papers I and II. This is still lower than what was reported by Stern et al. (2012) for candidates selected using the WISE colors. We believe the lower yields are mainly caused by the poor observing conditions or the non-uniform performance of the 4000 fibers of LAMOST.

### 4.2 Magnitude and Redshift Distributions

The magnitude limit of this sample is $i = 20.0$ mag. Among the 1330 newly discovered quasars, there are 15/35/84 new quasars with $i$-band magnitude brighter than 17.0/17.5/18.0 mag, respectively. Among the quasars discovered using the commissioning and pilot survey observations (Papers I and II), there are 6/21/81 quasars brighter than the aforementioned magnitude limits. Among the 75 quasars discovered by SDSS in the three spectroscopic plates in the outer halo of M31 (Adelman-McCarthy et al. 2006, 2007) and the 43 serendipitously discovered quasars in the two SEGUE plates

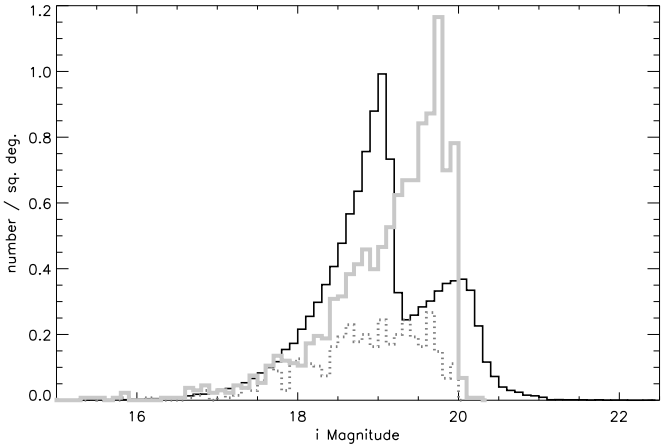


**Fig. 4** Histogram distribution of $i$-band magnitudes of the 1503 quasars detected by LAMOST in 2013 (*grey thick line*), including 1330 newly discovered and 173 previously detected by LAMOST. For comparison, the distribution of the 532 quasars detected by LAMOST in 2011 (*grey dotted line*), and that of SDSS DR7 quasars (Schneider et al. 2010; *black solid line*) are also plotted for comparison. The magnitude bin size is set to 0.1 mag. The $y$-axis gives the quasar number density per square degree.

of this field, the corresponding numbers are 0/1/6. Also, there are 24/41/54 quasars brighter than 17.0/17.5/18.0 mag in terms of $i$-magnitudes respectively, within 10 degrees of M31 and M33 in the NED archive (see Paper II). There are in total 45/98/225 quasars with $i$ magnitudes brighter than 17.0, 17.5 and 18.0 mag in this area, respectively. These bright quasars will be an invaluable sample to probe the properties of the ISM/IGM in M31/M33 and the Local Group.

Figure 4 shows the magnitude distribution of the 1503 quasars detected in the 2013 datasets, including the 1330 newly discovered and 173 cases that were previously known but re-observed by LAMOST. The magnitude has a bin size of 0.1 mag and the $y$-axis is given in quasar number density. For comparison, we also plot the $i$-band magnitude distribution of the 532 quasars detected by LAMOST in 2011 (Paper II), and the magnitude distribution of SDSS DR7 quasars (Schneider et al. 2010). We can see that there is a significant improvement in quasar number density by LAMOST in 2013 compared to that of 2011. It is difficult to compare our distribution directly with that of SDSS, given the different target selection algorithms. It is however clear that there are still a number of quasars that remain to be identified by LAMOST. This is also suggested by the relatively low efficiency of quasar identification by LAMOST, as pointed out above.

Figure 5 shows the redshift distribution of the 1503 quasars detected by LAMOST in 2013. The redshift has a bin size of 0.1. The $y$-axis gives quasar number density per square degree, as in Figure 4. The spectra of quasars with the lowest and highest redshift, J004342.5+372519.9 and J012220.3+345658.4 respectively, are shown in Figure 2. The second highest redshift is $z = 3.85$, and there are 41 quasars with redshifts higher than 3.0 in this new catalog.

In Figure 5, we also plot the redshift distribution of the 532 quasars detected by LAMOST in 2011 (Paper II), and the redshift distribution of SDSS DR7 quasars (Schneider et al. 2010), for comparison. We can see that there is a significant improvement in the number density of quasars detected by LAMOST in 2013 compared to that of 2011. In some redshift ranges, for example between 2.0 and 3.0, the number density of quasars identified by LAMOST is relatively higher than that of SDSS DR7. This is due to the different target selection algorithms adopted. Our targets include candidates

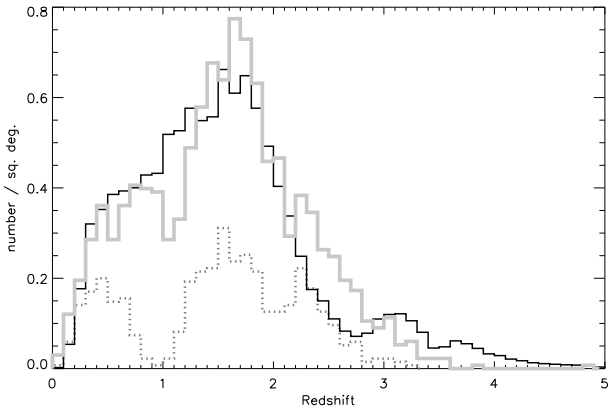


**Fig. 5** Redshift distribution of the 1503 quasars discovered by LAMOST in 2013 (*grey thick line*). The *grey dotted line* represents the redshift distribution of the 532 quasars discovered by LAMOST in 2011. The redshift distribution of the SDSS DR7 quasars (Schneider et al. 2010; *solid black line*) is also shown for comparison. The relatively low number density at $z \sim 2.7$ seen in the distribution of SDSS quasars is caused by the degeneracy in colors of stars and quasars around this redshift. The redshift bin size is set to 0.1. The $y$-axis gives the quasar number density per square degree.

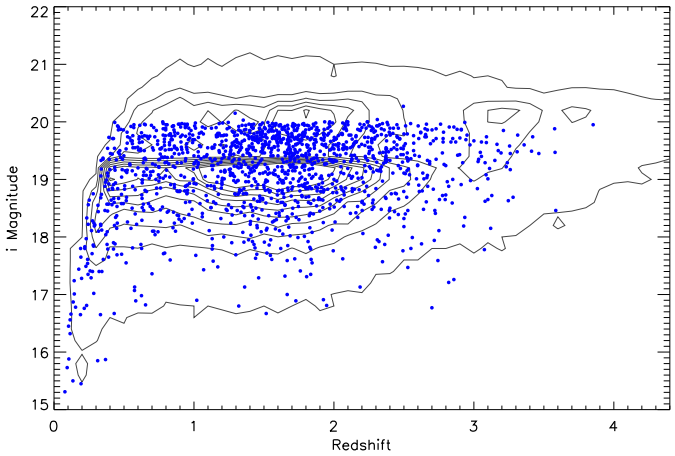


**Fig. 6** Redshift versus $i$-band magnitude distribution of the 1503 quasars detected by LAMOST in 2013 (*points*). The grey contours represent the redshift versus $i$-band magnitude distribution of the SDSS DR7 quasars (Schneider et al. 2010). The steep gradients near $i \approx 19.1$ and $i \approx 20.2$ mag are due to the magnitude limits of the SDSS selection algorithms for low- and high-redshift quasars, respectively. The relatively low number density at $z \sim 2.7$ is caused by the degeneracy of the SDSS colors of stars and quasars near this redshift.

selected with the WISE IR colors, thus increasing the probability of finding quasars with redshifts up to $z < 3.5$ (Wu et al. 2012). For redshifts of $z \leq 1.3$ or $z \geq 3.0$, the number density of quasars identified by LAMOST is lower than that of SDSS. The selection effects in the redshift distribution of quasars detected in 2013 are not as severe as those of 2011. The distribution of quasars discovered in 2011 has two obvious troughs in redshift, one near redshift $\sim 0.9$ and the other near $\sim$2.1 (see Paper

II for details). This improvement has benefitted from improvements in the performance of LAMOST as well as in the 2D pipeline. Figure 6 shows the distribution of quasars in the redshift-magnitude plane detected by LAMOST in 2013. The distribution is concentrated near redshifts between 1.2 and 2.0, and $i$ magnitudes between 19.0 and 20.0. This is also apparent in Figures 4 and 5. Given the heterogeneous target selection algorithms and the relatively low efficiency of identification, this sample is not intended for the purpose of statistical analysis.

**Acknowledgements** This work is supported by the National Key Basic Research Program of China (2014CB845705) and the National Natural Science Foundation of China (NSFC, Grant No. 11403038). We thank the staff of Lijiang Observatory, which is administered by Yunnan Observatories, for the observations and technical support, particularly Jin-Ming Bai and Wei-Min Yi, as well as help from Hong-Liang Yan from National Astronomical Observatories, Chinese Academy of Sciences. The Guo Shou Jing Telescope (the Large Sky Area Multi-Object Fiber Spectroscopic Telescope, LAMOST) is a National Major Scientific Project built by the Chinese Academy of Sciences. Funding for the project has been provided by the National Development and Reform Commission. LAMOST is operated and managed by National Astronomical Observatories, Chinese Academy of Sciences.

Funding for the SDSS and SDSS-II has been provided by the Alfred P. Sloan Foundation, the Participating Institutions, the National Science Foundation, the U.S. Department of Energy, the National Aeronautics and Space Administration, the Japanese Monbukagakusho, the Max Planck Society, and the Higher Education Funding Council for England. The SDSS Web Site is *http://www.sdss.org/*.

This publication makes use of data products from the Wide-field Infrared Survey Explorer, which is a joint project of the University of California, Los Angeles, and the Jet Propulsion Laboratory/California Institute of Technology, funded by the National Aeronautics and Space Administration.

This research has made use of the NASA/IPAC Extragalactic Database (NED) which is operated by the Jet Propulsion Laboratory, California Institute of Technology, under contract with the National Aeronautics and Space Administration.

## References

Adelman-McCarthy, J. K., Agüeros, M. A., Allam, S. S., et al. 2006, ApJS, 162, 38
Adelman-McCarthy, J. K., Agüeros, M. A., Allam, S. S., et al. 2007, ApJS, 172, 634
Binney, J., & Tremaine, S. 1987, Galactic dynamics (Princeton: Princeton Univ. Press)
Boyle, B. J., Shanks, T., Croom, S. M., et al. 2000, MNRAS, 317, 1014
Brunthaler, A., Reid, M. J., Falcke, H., Greenhill, L. J., & Henkel, C. 2005, Science, 307, 1440
Corbett, E. A., Croom, S. M., Boyle, B. J., et al. 2003, MNRAS, 343, 705
Cui, X.-Q., Zhao, Y.-H., Chu, Y.-Q., et al. 2012, RAA (Research in Astronomy and Astrophysics), 12, 1197
Darling, J. 2011, ApJ, 732, L2
de Vaucouleurs, G., de Vaucouleurs, A., Corwin, Jr., H. G., et al. 1991, Third Reference Catalogue of Bright Galaxies. Volume I: Explanations and References. Volume II: Data for Galaxies between $0^h$ and $12^h$. Volume III: Data for Galaxies between $12^h$ and $24^h$. (New York: Springer)
Dorman, C. E., Guhathakurta, P., Fardal, M. A., et al. 2012, ApJ, 752, 147
Gebhardt, K., Bender, R., Bower, G., et al. 2000, ApJ, 539, L13
Gilbert, K. M., Guhathakurta, P., Kollipara, P., et al. 2009, ApJ, 705, 1275
Gilbert, K. M., Guhathakurta, P., Beaton, R. L., et al. 2012, ApJ, 760, 76
Gilbert, K. M., Kalirai, J. S., Guhathakurta, P., et al. 2014, ApJ, 796, 76
Huchra, J. P., Brodie, J. P., & Kent, S. M. 1991, ApJ, 370, 495
Huo, Z.-Y., Liu, X.-W., Yuan, H.-B., et al. 2010, RAA (Research in Astronomy and Astrophysics), 10, 612

Huo, Z.-Y., Liu, X.-W., Xiang, M.-S., et al. 2013, AJ, 145, 159
Ibata, R., Martin, N. F., Irwin, M., et al. 2007, ApJ, 671, 1591
Jester, S., Schneider, D. P., Richards, G. T., et al. 2005, AJ, 130, 873
Liu, X.-W., Yuan, H.-B., Huo, Z.-Y., et al. 2014, in IAU Symposium, 298, eds. S. Feltzing, G. Zhao, N. A. Walton, & P. Whitelock, 310
Liu, X. W., Zhao, G., & Hou, J. L. 2015, RAA (Research in Astronomy and Astrophysics), 15, 1089
Loeb, A., Reid, M. J., Brunthaler, A., & Falcke, H. 2005, ApJ, 633, 894
Luo, A.-L., Zhang, Y.-X., & Zhao, Y.-H. 2004, in Society of Photo-Optical Instrumentation Engineers (SPIE) Conference Series, 5496, Advanced Software, Control, and Communication Systems for Astronomy, eds. H. Lewis & G. Raffi, 756
Luo, A.-L., Zhang, H.-T., Zhao, Y.-H., et al. 2012, RAA (Research in Astronomy and Astrophysics), 12, 1243
Luo, A.-L., Zhao, Y.-H., Zhao, G., et al. 2015, RAA (Research in Astronomy and Astrophysics), 15, 1095
Massey, P., Olsen, K. A. G., Hodge, P. W., et al. 2006, AJ, 131, 2478
McConnachie, A. W., Irwin, M. J., Ferguson, A. M. N., et al. 2005, MNRAS, 356, 979
McConnachie, A. W., Irwin, M. J., Ibata, R. A., et al. 2009, Nature, 461, 66
Murdoch, H. S., Hunstead, R. W., Pettini, M., & Blades, J. C. 1986, ApJ, 309, 19
Pâris, I., Petitjean, P., Aubourg, É., et al. 2012, A&A, 548, A66
Pâris, I., Petitjean, P., Aubourg, É., et al. 2014, A&A, 563, A54
Rao, S. M., Sardane, G., Turnshek, D. A., et al. 2013, MNRAS, 432, 866
Richards, G. T., Fan, X., Newberg, H. J., et al. 2002, AJ, 123, 2945
Savage, B. D., Wakker, B., Jannuzi, B. T., et al. 2000, ApJS, 129, 563
Schlegel, D. J., Finkbeiner, D. P., & Davis, M. 1998, ApJ, 500, 525
Schmidt, M. 1963, Nature, 197, 1040
Schneider, D. P., Hartig, G. F., Jannuzi, B. T., et al. 1993, ApJS, 87, 45
Schneider, D. P., Richards, G. T., Hall, P. B., et al. 2010, AJ, 139, 2360
Sohn, S. T., Anderson, J., & van der Marel, R. P. 2012, ApJ, 753, 7
Stern, D., Assef, R. J., Benford, D. J., et al. 2012, ApJ, 753, 30
Su, D.-Q., & Cui, X.-Q. 2004, ChJAA (Chin. J. Astron. Astrophys.), 4, 1
Tollerud, E. J., Beaton, R. L., Geha, M. C., et al. 2012, ApJ, 752, 45
van der Marel, R. P., & Guhathakurta, P. 2008, ApJ, 678, 187
Walterbos, R. A. M., & Kennicutt, Jr., R. C. 1987, A&AS, 69, 311
Wang, S.-G., Su, D.-Q., Chu, Y.-Q., Cui, X., & Wang, Y.-N. 1996, Appl. Opt., 35, 5155
Wright, E. L., Eisenhardt, P. R. M., Mainzer, A. K., et al. 2010, AJ, 140, 1868
Wu, X.-B., Hao, G., Jia, Z., Zhang, Y., & Peng, N. 2012, AJ, 144, 49
Yan, L., Donoso, E., Tsai, C.-W., et al. 2013, AJ, 145, 55
Yanny, B., Rockosi, C., Newberg, H. J., et al. 2009, AJ, 137, 4377
York, D. G., Adelman, J., Anderson, Jr., J. E., et al. 2000, AJ, 120, 1579
Yuan, H.-B., Liu, X.-W., Huo, Z.-Y., et al. 2015, MNRAS, 448, 855
Zhao, G., Zhao, Y.-H., Chu, Y.-Q., Jing, Y.-P., & Deng, L.-C. 2012, RAA (Research in Astronomy and Astrophysics), 12, 723